Journal of the Optical Society of America B
OPTICAL PHYSICS

Diffraction-free distance enhancement of Bessel beams based on spatial domain phase modulation

Chengming Lyu,[1] Yiqi Zhang,[1,3] Milivoj R. Belić,[2] Yongdong Li,[1] and Yongfeng Kang[1,4]

[1]Key Laboratory for Physical Electronics and Devices of the Ministry of Education & Shaanxi Key Lab of Information Photonic Technique, School of Electronic Science and Engineering, Xi'an Jiaotong University, Xi'an 710049, China
[2]Science Program, Texas A&M University at Qatar, Doha, P.O. Box 23874, Qatar
[3]zhangyiqi@mail.xjtu.edu.cn
[4]yfkang@mail.xjtu.edu.cn

Received 10 August 2023; revised 23 September 2023; accepted 3 October 2023; posted 3 October 2023; published 23 October 2023

Bessel beams have garnered significant interest due to their unique diffraction-free properties and extensive potential applications. In this work, we propose a spatial domain phase modulation theory to achieve diffraction-free distance enhancement of Bessel beams, overcoming the limitation of the traditional methods due to the inability to infinitely decrease the wave vector angle. The traditional formula for non-diffraction distance is also modified. Simulation results demonstrate that our proposed scheme can significantly increase the maximum diffraction-free distance of zero-order and higher-order Bessel beams by more than two times, while ensuring the self-healing property of Bessel beams. Furthermore, our proposed scheme is not restricted to specific systems or limited to the optical wavelength range. This implies that the results have great applicative potential in long-distance free-space optical communication and wireless energy transmission.

https://doi.org/10.1364/JOSAB.502991

1. INTRODUCTION

The diffraction-free beam is a unique type of beam that undergoes no diffraction upon propagation in free space. Among the earliest known examples of this phenomenon are Bessel beams [1]. The Bessel beam is a solution to the three-dimensional Helmholtz equation, whereby its field distribution in the transverse plane (x, y) is determined by the first kind of Bessel functions, while the longitudinal coordinate (z) denotes the direction of propagation. Remarkably, this beam sustains a constant intensity distribution and possesses a highly localized intensity profile during propagation. Subsequently, with the development of laser technology and expansion of its application fields, some other non-diffracting beams such as the Mathieu beam [2] and parabolic beam [3] have been proposed and extensively researched in recent years. Moreover, by considering the paraxial approximation for the Helmholtz equation, which yields the Schrödinger-like equation, Berry and Balazs found the Airy non-diffracting wavepacket [4]. Based on this, Christodoulides' group created finite-energy Airy beams [5,6] that accelerate along a parabolic trajectory, thereby opening a new chapter in the history of diffraction-free self-accelerating beams. Similarly, since an ideal diffraction-free Bessel beam requires an infinite amount of energy, Bessel beams of finite transverse size can only remain diffraction-free over a certain range, so they are strictly defined as quasi-diffraction-free. Throughout this paper, all the phrases "diffraction-free" refer to quasi-diffraction-free. So far, potential applications of Bessel beams have been demonstrated in optical trapping [7,8], laser drilling [9], laser precision collimation [10], optical coherence tomography [11,12], micro-manipulation [13], and wireless power transmission [14]. In addition to the non-diffracting characteristics, when part of the beam is blocked by an obstacle, the Bessel beam can self-reconstruct its field [15,16], which is known as the self-healing property, thereby providing an effective solution for long-distance free-space optical communication [17–19]. In recent years, the self-accelerating property of the Bessel beam has been inspected seriously [20–22].

In 1987, Durnin employed the ring-slit method to generate approximate Bessel beams within a finite distance in experiments, which can maintain the propagation of the main lobe without broadening in the non-diffraction range [1]. The essence of the formation of Bessel beams lies in that Bessel beams can be expressed as a superposition of plane waves, where all the plane waves have the same inclination angle with respect to the propagation axis but different azimuthal angles ranging from 0 to 2π, i.e., the wave vectors are distributed over a cone, which can be synthesized by an axicon, called the axicon model [23]. Most methods of generating Bessel beams, such as computer-generated holograms [24], combined axicons [25], volume holographic axicons [26], metasurfaces [27–29], diffraction gratings [30], toroidal (annular) lenses, [31] and spatial light modulators [32–35], are regarded to be equivalent to the axicon

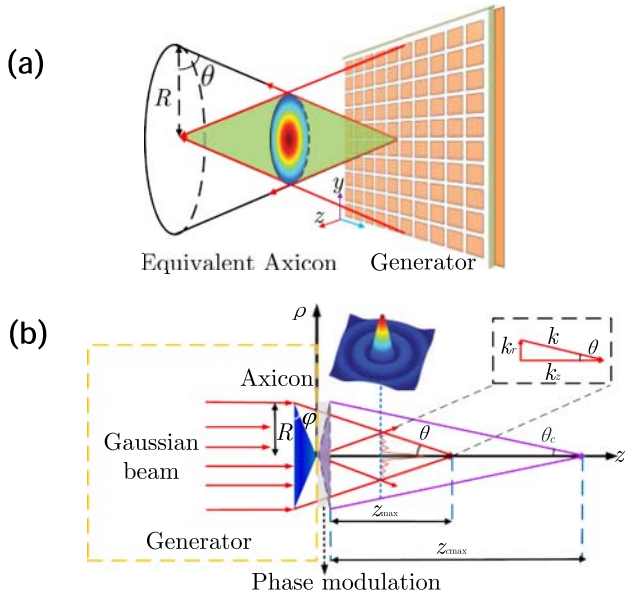

Fig. 1. (a) Equivalent axicon model. (b) Schematic diagram of phase modulation. R is the radius of the axicon, φ is the base angle of the axicon, θ is the wave vector angle, θ_c is the modulated wave vector angle, $z_{\max}$ is the maximum diffraction-free distance (red lines), and $z_{c\,\max}$ is the corrected maximum diffraction-free distance (purple lines). The blue axicon is an equivalent model to the Bessel generator, and the purple axicon is the equivalent virtual axicon model for spatial phase modulation.

model [see Fig. 1(a)]. Therefore, we adopt the axicon model to replace the Bessel beam generator. Figure 1(b) shows a Gaussian beam vertically incident on an axicon with a base angle of φ and an aperture radius of R. The axicon converts the incident beam into a diffraction field on the right-hand side, and the interference of the diffracted waves generates a diffraction-free Bessel beam with a wave vector angle of θ. Bessel beams exhibit diffraction-free and self-healing properties within a maximum non-diffracting distance $z_{\max}$. From the geometric relationship in Fig. 1, we obtain [23]

$$z_{\max} = \frac{R}{\tan\theta}, \tag{1}$$

with $\theta = (n-1)\varphi$, where n is the refractive index of the axicon. As a result, the $z_{\max}$ increases with the increase in R and decrease in θ. However, R cannot infinitely increase to its ideal value, and θ cannot infinitely reduce due to technological and material limitations. Consequently, the utilization of Bessel beams in engineering applications is impeded by their limitation of only maintaining non-diffracting characteristics within a short propagation distance. Therefore, it is imperative to investigate and devise methods that can augment the non-diffracting range beyond the existing constraints. Efforts in this direction demand a comprehensive exploration of the key factors that determine the non-diffracting range of Bessel beams while maintaining compatibility with existing systems.

In this study, we propose a novel theory of spatial domain phase modulation that offers a promising solution for improving the non-diffracting distance of both zero-order and higher-order Bessel beams. Our approach involves manipulating the angular spectrum of Bessel beams in the frequency domain by applying spatial domain phase modulation, which effectively circumvents the limitations imposed by material or technological constraints on the wave vector angles. Importantly, our approach is not restricted by wavelength requirements and can be implemented using readily available spatial light modulators or metamaterials [36,37], which is expected to significantly enhance the practicality and accessibility of our technique. By integrating our method with existing approaches, we aim to achieve improved performance in various applications, such as long-distance wireless energy transfer, free-space optical communication, remote sensing, and more. Our work demonstrates the versatility and efficacy of spatial domain phase modulation as a means of optimizing the performance of non-diffracting beams. We anticipate that our findings will inspire further research in this area and lead to the development of advanced optical systems that can exploit the full potential of Bessel beams.

2. RESULTS AND DISCUSSION

A. Spatial Domain Phase Modulation Theory

As shown in Fig. 2, the frequency domain distribution of the spatial domain distribution $f(r)$ is defined as $F(\rho)$, which is the Fourier transform of $f(r)$, where r is the spatial domain position and ρ is the corresponding frequency domain position. The spatial domain after phase modulation is given by $f(r)e^{i2\pi cr}$, where c is referred to as the modulation factor in m^{-1} and i is an imaginary unit. Then the distribution of the frequency domain after phase modulation is $\mathcal{F}\{f(r)e^{i2\pi cr}\}$, where $\mathcal{F}$ is the Fourier transform operator. According to the property of Fourier transform, the spatial domain product is equivalent to the convolution in the frequency domain, so one can obtain

$$\mathcal{F}\{f(r)e^{i2\pi cr}\} = \mathcal{F}\{f(r)\} * \delta(\rho + c), \tag{2}$$

where $*$ is the convolution operator. Let

$$f(r) = J_0(\alpha r), \tag{3}$$

where J_0 represents the zero-order Bessel function. $\alpha = k\sin\theta$, with $k = 2\pi/\lambda$ being wavenumber, λ is the wavelength, and θ is the wave vector angle. Substituting Eq. (3) into Eq. (2), one gets

$$\mathcal{F}\{f(r)e^{i2\pi cr}\} = \frac{1}{2\pi\rho_0}\delta(\rho - \rho_c), \tag{4}$$

where δ is the impulse function that is expressed as an angular spectrum ring in the frequency domain, $\rho_0 = \alpha/2\pi$ is the radius of the Bessel angular spectrum ring, and $\rho_c = \rho_0 - c = \alpha_c/2\pi$ is the radius of the Bessel angular spectrum ring after spatial domain phase modulation. As illustrated in Fig. 2, the radius of the Bessel angle spectrum decreases by exerting phase modulation in the spatial domain. The wave vector angle without phase modulation is $\theta = \arcsin(\alpha/k)$, and the wave vector angle after applying phase modulation in the spatial domain is given by

$$\theta_c = \arcsin\left(\frac{\alpha_c}{k}\right) = \arcsin(\sin\theta - \lambda c). \tag{5}$$

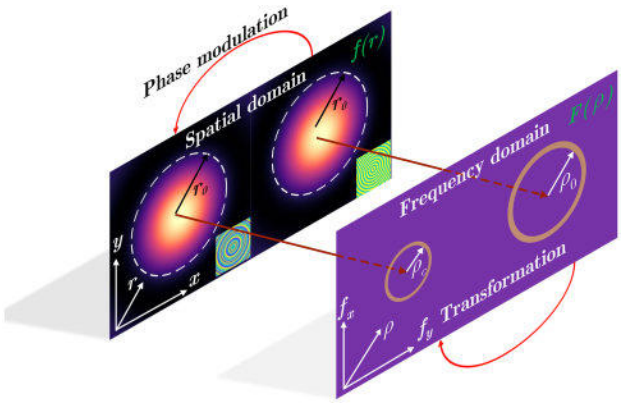

Fig. 2. Space domain phase modulation theory. The reduction of the radius of the Bessel angular spectrum ring in the frequency domain is achieved by implementing phase modulation in the spatial domain.

Thus, Eq. (1) is corrected to

$$z_{c\ \max} = \frac{R}{\tan\theta_c} = \frac{R}{\tan[\arcsin(\sin\theta - \lambda c)]}. \tag{6}$$

$z_{c\ \max}$ is the corrected maximum diffraction-free distance. If θ is a small angle, Eq. (6) can be written as

$$z_{c\ \max} = \frac{R}{\theta - \lambda c}. \tag{7}$$

Consequently, the diffraction-free distance will increase significantly, as illustrated in Fig. 1(b), where the red lines represent no phase modulation and the purple lines represent applied phase modulation. The essence of spatial phase modulation is to transform the angular spectrum ring by applying phase modulation, which benefits from the fact that the modulation function $e^{i2\pi cr}$ behaves as a sampling impulse function δ in the frequency domain. Since the axicon has an equal effect on Gaussian beams, spatial phase modulation applied on a spatial light modulator or metasurface can be equivalent to a virtual axicon, as shown by the purple axicon in Fig. 1(b), from the perspective of the resulting transformation. From Eqs. (5) and (7), we can notice that θ and $z_{\max}$ are only special cases of θ_c and $z_{c\ \max}$ in the case $c = 0$. Therefore, we uniformly express the maximum diffraction-free distance as $z_{\max}$ and the wave vector angle as θ in the following text.

B. Diffraction-Free Distance Enhancement

Next, we consider Bessel beams generated from axicon model. The parameters are as follows: $\lambda = 632.8$ nm, $R = 2.5$ mm, $n = 1.5$, $\varphi = 0.2°$, $\theta = 0.1°$. Note that this wave vector angle is highly demanding for material processing. The intensity and phase distributions of the original unmodulated zero-order Bessel beams are shown in Fig. 3(a), where the phase distribution has only two discrete values of 0 and π. Figure 3(b) presents the phase masks at different values of c, which can be loaded onto a spatial light modulator or metasurface to conveniently manipulate the phase of the original Bessel beams. Figure 3(c) depicts the phase distribution obtained after spatial domain phase modulation, which does not exhibit any readily discernible regularities. Therefore, a frequency domain analysis is essential

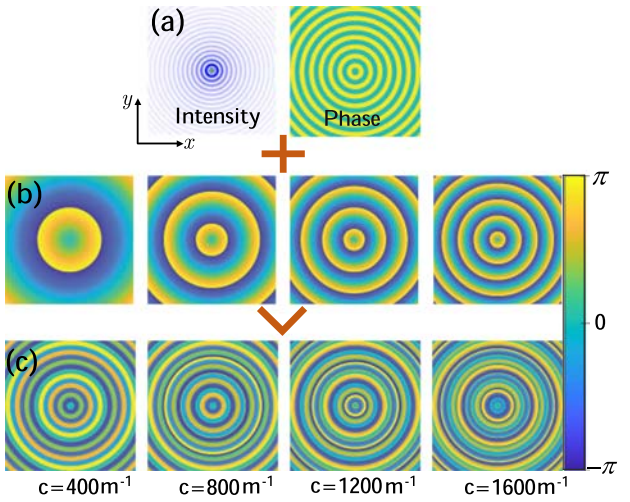

Fig. 3. (a) Transverse intensity and phase distributions of the original zero-order Bessel beam. (b) Modulation phase mask with different modulation factor c. (c) Phase distributions after phase modulation. Panels in each column in (b) and (c) have the same c. All panels are shown in the window $-2.5\ \text{mm} \le x, y \le 2.5\ \text{mm}$.

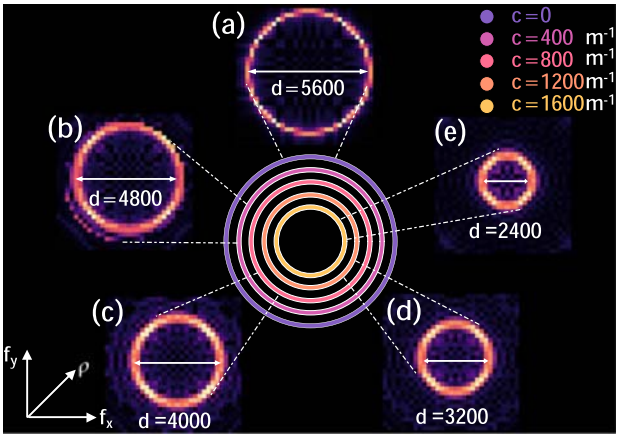

Fig. 4. Frequency domain distributions of the Bessel beams, which has been modulated by spatial phase in the respective cases of (a) $c = 0$, (b) $c = 400\ \text{m}^{-1}$, (c) $c = 800\ \text{m}^{-1}$, (d) $c = 1200\ \text{m}^{-1}$, and (e) $c = 1600\ \text{m}^{-1}$. As the modulation factor c increases, the width of the Bessel angular spectrum ring in the frequency domain decreases. Note that, for the convenience of displaying the spectral ring variation, we did not label the symmetric parts of each ring in the figure. In fact, the frequency domain components are always symmetrically distributed.

for uncovering any underlying structures. Figures 4(a)–4(e) depict the frequency domain distributions for $c = 0$, $400\ \text{m}^{-1}$, $800\ \text{m}^{-1}$, $1200\ \text{m}^{-1}$, and $1600\ \text{m}^{-1}$, respectively. As anticipated, the Bessel beam is observed to form an angular spectrum ring, and the width of the ring linearly decreases from 5600/m to 2400/m as c increases. This implies that we have achieved a scaling transformation of the Bessel beam's angular spectrum ring through spatial domain phase modulation. Since the width of the Bessel angular spectrum ring is proportional to $\alpha = k\sin\theta$ (ring width $= \alpha/2\pi$), the reduction of the wave vector angle θ leads to a significant improvement in its diffraction-free ability.

We have implemented the simulation of Bessel beam propagation based on the angular spectrum propagation theory [25]. The field distribution at z in the real space is

$$\psi_p = \mathcal{F}^{-1}\{\mathcal{F}\{\psi_{p0}(x, y)\} \cdot \mathcal{H}(k_x, k_y; z)\}, \tag{8}$$

where $\mathcal{F}$ and $\mathcal{F}^{-1}$ are the Fourier transform operator and its inverse, respectively, and ψ_{p0} is the initial field distribution. We refer to $\mathcal{H}$ as the spatial frequency transfer function at the position z to which the light has traveled in the medium. $\mathcal{H}$ is given by

$$\mathcal{H} = e^{ikz} \exp[-i\pi\lambda z(f_x^2 + f_y^2)], \tag{9}$$

where k is the wavenumber. λ is the wavelength, where $k = 2\pi/\lambda$, with λ being the wavelength in the medium, and $f_x = k_x/2\pi$ and $f_y = k_y/2\pi$ are the coordinate variables in the frequency domain.

In Fig. 5(a), the intensity distribution of the beam propagation in the (xoz) plane is shown for modulation factors $c = 0$ (no modulation), $c = 400\ \mathrm{m}^{-1}$, $c = 800\ \mathrm{m}^{-1}$, $c = 1200\ \mathrm{m}^{-1}$, and $c = 1600\ \mathrm{m}^{-1}$, where the red triangle marks the maximum diffraction-free distance. It can be observed that, as the modulation factor c increases, the maximum diffraction-free distance significantly increases and exhibits an accelerating growth trend. The evolution of the axial intensity of the zero-order Bessel beam is shown in Fig. 5(b), which further verifies this achievement. The maximum diffraction-free distance is defined as the propagation distance where the axial intensity decreases to half of its original value. As indicated by the horizontal brown dashed line, it can be clearly found that, the larger the value of c is, the larger the $z_{\max}$ is. The theoretical and simulated values of the diffraction-free distance are listed in the second and third columns of Table 1, respectively, revealing a good agreement between the theoretical calculations and simulations. The fourth column lists the percentage of the distance improvement, and when $c = 1600\ \mathrm{m}^{-1}$, the distance increases by more than twice. As c continues to increase, this value will further escalate. Accordingly, the diffraction-free distance will increase by a factor of two or more for different Bessel beam generation systems with the appropriate modulation factor c. However, it is crucial to note that an excessively large value of c will lead to a degradation in beam quality. Hence, it is recommended to restrict the value of c to be less than $2\theta/3\lambda$. When c is set to $1200\ \mathrm{m}^{-1}$, the intensity distribution of the zero-order Bessel beam in the (xoy) plane at different distances is presented in Fig. 5(e). It is evident that, within the $z_{\max}$, the main lobe width remains unchanged during propagation. However, when the distance z exceeds $z_{\max}$, the energy of the main lobe starts to extend into the side lobes, and the side lobes gradually become visible. Figure 5(c) illustrates the variation of the main lobe width w of a Bessel beam during propagation under different modulation factors c. It is worth noting that the main lobe width after phase modulation is not the same. This can be easily explained by the fact that the main lobe width can be calculated using $2.405/\alpha$. Therefore, as the modulation factor c increases, θ and α decrease, and the main lobe width increases accordingly. Correspondingly, as illustrated in Fig. 5(d), the percentage of the main lobe power of the zeroth-order Bessel beam also increases, indicating that, as the parameter "c" increases, the percentage of power within the main lobe proportionally rises. To be more precise, the implementation of phase modulation involves a process of formation, graphically denoted by the red dashed line on Fig. 5(c), whereby the left side represents the formative stage and the right side indicates the lack of diffraction. However, this does not affect the ability of the Bessel beam to remain diffraction-free over a relatively long propagation distance along the z direction.

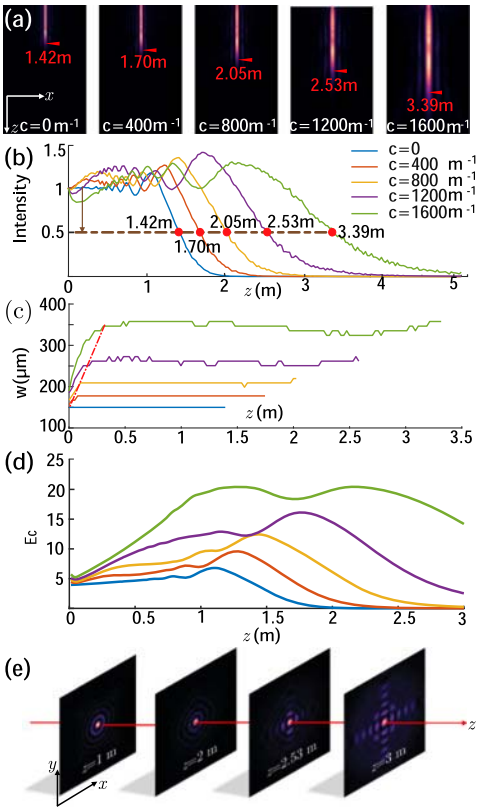

Fig. 5. (a) Propagation intensity of the zero-order Bessel beam at different modulation factors c, with the maximum diffraction-free distance $z_{\max}$ marked by red triangles. (b) Peak intensity; the crossing point with the brown dashed line is $z_{\max}$. (c) Main lobe width of Bessel beams during propagation with different modulation factors c. The red dashed line divides the formation process from the diffraction-free process. (d) The main lobe power percentage of the Bessel beam at different modulation factors c. E is the main lobe power percentage (%). (e) Intensity distributions at different distances with $c = 1200\ \mathrm{m}^{-1}$ and $z_{\max} = 2.53$ m. (b)–(d) have the same legend. Panels in (a) are shown in $-2.5\ \mathrm{mm} \le x \le 2.5\ \mathrm{mm}$, $0\ \mathrm{m} \le z \le 5\ \mathrm{m}$. Panels in (e) are shown in $-2.5\ \mathrm{mm} \le x, y \le 2.5\ \mathrm{mm}$.

Table 1. Comparison between Theoretical Results and Simulations on the Maximum Diffraction-Free Distance[a]

$c(\mathrm{m}^{-1})$	Theory (m)	Simulation (m)	*Dis*
0	1.4331	1.4174	0
400	1.6764	1.6959	19.6%
800	2.0191	2.0503	44.7%
1200	2.5379	2.5312	78.6%
1600	3.4155	3.3918	139.3%

[a]*Dis* is the distance improvement percentage.

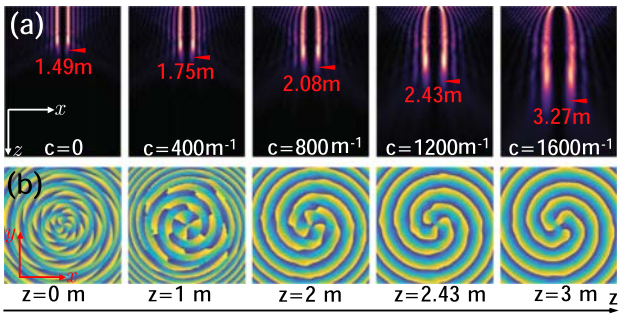

Fig. 6. (a) Setup is as Fig. 5(a), but for the high-order Bessel beam ($l = 3$). (b) Phase distribution of the high-order Bessel beam with $c = 1200\ \mathrm{m}^{-1}$ at different distances. Panels in (a) are shown in $-2.5\ \mathrm{mm} \le x \le 2.5\ \mathrm{mm}$, $0\ \mathrm{m} \le z \le 5\ \mathrm{m}$. Panels in (b) are shown in $-2.5\ \mathrm{mm} \le x, y \le 2.5\ \mathrm{mm}$.

As a result, the implementation of phase modulation allows for an increase in the maximum diffraction-free distance of the Bessel beam. Furthermore, this approach is not limited to the specific generation method of the Bessel beam nor is it restricted solely to the optical frequency range. Therefore, this method represents a promising solution for long-range wireless energy transfer using either laser or microwave radiation.

Now, we demonstrate that this method is also feasible to higher-order Bessel beams, which are a class of vortex waves whose expressions are $J_l(\alpha r)e^{il\phi}$, where l is referred to as the topological charge (i.e., the order of the Bessel beam) and ϕ as the azimuthal angle [38,39]. Although our theoretical derivation is based on zero-order Bessel beams, this method also exhibits similar results in high-order Bessel beams. As shown in Fig. 6(a), we present the intensity distribution of a third-order Bessel beam propagation [(xoz) plane]. Similar to the conclusion of the zero-order Bessel beam, as the value of c increases, its maximum diffraction-free distance gradually increases, and the difference in $z_{\max}$ with the zero-order Bessel beam is not significant. Moreover, the higher-order Bessel beam also expands within an extremely short distance and then maintains a constant main lobe width over a long range. Given that higher-order Bessel beams carry orbital angular momentum, they can be employed for free-space optical communication. Hence, it is crucial to investigate the phase distribution. Taking $c = 1200\ \mathrm{m}^{-1}$, the phase evolution during its propagation is shown in Fig. 6(b). As the propagation distance increases, the phase distribution becomes more ordered. It is noteworthy that the topological charge carried by a Bessel beam represents the phase variation occurring within one azimuthal period around the beam axis. For instance, a Bessel beam of the third order carries a topological charge of 3, indicating three 2π phase variations happening in one azimuthal period. As a result, it can be observed from Fig. 6(b) that the information conveyed by the Bessel beam can still be decoded even if the distance exceeds the maximum diffraction-free distance of 2.43 m. To conclude, the spatial domain phase modulation scheme can effectively enhance the diffraction-free distance of zero-order and higher-order Bessel beams. The idea underlying this scheme is to apply phase modulation in the spatial domain, which can be achieved quite simply by spatial light modulators [40,41] or metasurfaces [42–46], and is experimentally achievable with little difficulty.

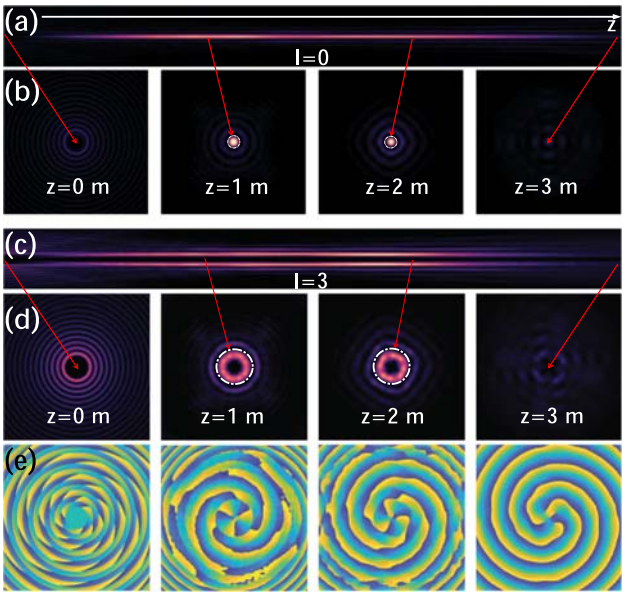

Fig. 7. (a) Intensity distribution of the zero-order Bessel beam in the xoz plane with the main lobe removed when $c = 1200\ \mathrm{m}^{-1}$. (b) Propagation intensity distributions at different propagation distances. (c), (d) Setup is as (a), (b) but for the high-order Bessel beam ($l = 3$). (e) Phase distribution corresponding to (d). Panels in (a), (c) are shown in $-2.5\ \mathrm{mm} \le x \le 2.5\ \mathrm{mm}$, $0\ \mathrm{m} \le z \le 3\ \mathrm{m}$. Panels in (b), (d), (e) are shown in $-2.5\ \mathrm{mm} \le x, y \le 2.5\ \mathrm{mm}$. The recovered main lobe is indicated by the white dotted circles.

C. Self-Healing Property

One of the noteworthy characteristics exhibited by diffraction-free beams is their self-healing capability [47], which can also be observed in Bessel beams created based on spatial domain phase modulation. Figures 7(a) and 7(c) illustrate the transverse intensity distributions of the zero-order Bessel beam and third-order Bessel beam, respectively, propagating along the z axis when $c = 1200\ \mathrm{m}^{-1}$. Figures 7(b) and 7(d) depict the corresponding intensity distributions in the (xoy) plane at $z = 0$ m, $z = 1$ m, $z = 2$ m, and $z = 3$ m, respectively. The Bessel beams after removing the main lobe are shown in the panels with $z = 0$. After propagating to $z = 1$ m, the main lobe appears to be restored by the energy from the side lobes; the white dashed circles represent the reconstructed main lobe. Furthermore, the main lobe is still present when it propagates to 2 m. The phase of the higher-order Bessel beams is also restored during propagation, which can be observed in Fig. 7(e).

As illustrated in Fig. 8, the blue and brown curves correspond to the normalized energy distribution within the primary lobe region of the zeroth-order and third-order Bessel beams, respectively, following the removing of the main lobe. E is the main lobe energy after normalization. It is evident that, during the initial period following the removal of the main lobe in a Bessel beam, the energy within the main lobe demonstrates a nearly linear growth trend as the beam propagates. This supports the notion that the Bessel beam is undergoing a rapid self-recovery process. Subsequently, the energy within the Bessel beam's main lobe remains above 0.5 for a defined duration, characterizing the "remain" phase of the Bessel beam. Ultimately, due to the influence of diffraction effects and surpassing the maximum

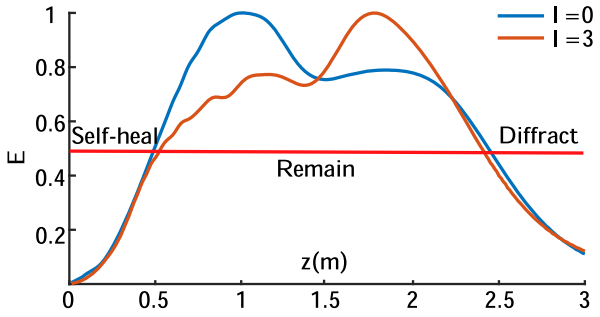

Fig. 8. Normalized main lobe energy of zero-order Bessel beams (brown line) and third-order Bessel beams (blue line) after obstacle occlusion when $c = 1200\ \mathrm{m}^{-1}$. E is the main lobe energy after normalization.

non-diffracting distance, the energy within the Bessel beam's main lobe diminishes, marking the onset of the "diffract" phase. Moreover, it is worth mentioning that the self-healing rates of the zeroth-order and third-order Bessel beams are essentially equivalent. For enhanced visualization, we have provided Visualization 1 and Visualization 2 that features animated depictions of the self-healing processes of the aforementioned beams [as the beam propagates, the main lobe (red) reappears].

3. CONCLUSION

In summary, we proposed a spatial domain phase modulation theory to generate long-range non-diffracting Bessel beams and provided a modified expression for the maximum diffraction distance. Furthermore, this method is applicable to both zero-order and higher-order Bessel beams. Simulation results show that, as the modulation factor increases and the wave vector angle decreases, the non-diffracting distance of the Bessel beam is correspondingly increased. Based on the parameter settings in this work, the diffraction-free distance of the Bessel beam can be up to 2.39 times the diffraction-free distance of the original Bessel beam after applying phase modulation in the spatial domain. In addition, we have also observed a reduction in the width of the Bessel angle spectrum ring in the frequency domain. The self-healing property of the Bessel beam is demonstrated by observing the reconstruction of the main lobe after removing the main lobe. Our method improves upon existing methods and is compatible with existing Bessel beam generation systems, making it highly versatile. Moreover, it is not limited to the optical waveband, suggesting that our work may serve as a reliable solution for long-distance wireless optical communication or energy transmission.

Funding. National Natural Science Foundation of China (12074308, U1537210); Qatar National Research Fund (NPRP 13S-0121-200126).

Disclosures. The authors declare no conflicts of interest.

Data availability. Data underlying the results presented in this paper are not publicly available at this time but may be obtained from the authors upon reasonable request.

REFERENCES

1. J. Durnin, J. J. Miceli, and J. H. Eberly, "Diffraction-free beams," Phys. Rev. Lett. **58**, 1499–1501 (1987).
2. J. C. Gutiérrez-Vega, M. D. Iturbe-Castillo, and S. Chávez-Cerda, "Alternative formulation for invariant optical fields: Mathieu beams," Opt. Lett. **25**, 1493–1495 (2000).
3. M. A. Bandres, J. C. Gutiérrez-Vega, and S. Chávez-Cerda, "Parabolic nondiffracting optical wave fields," Opt. Lett. **29**, 44–46 (2004).
4. M. V. Berry and N. L. Balazs, "Nonspreading wave packets," Am. J. Phys. **47**, 264–267 (1979).
5. G. A. Siviloglou and D. N. Christodoulides, "Accelerating finite energy Airy beams," Opt. Lett. **32**, 979–981 (2007).
6. G. A. Siviloglou, J. Broky, A. Dogariu, and D. N. Christodoulides, "Observation of accelerating Airy beams," Phys. Rev. Lett. **99**, 213901 (2007).
7. A. S. Desyatnikov, V. G. Shvedov, A. V. Rode, W. Krolikowski, and Y. S. Kivshar, "Photophoretic manipulation of absorbing aerosol particles with vortex beams: theory versus experiment," Opt. Express **17**, 8201–8211 (2009).
8. J. C. H. Spence, G. Subramanian, and P. Musumeci, "Hollow cone illumination for fast TEM, and outrunning damage with electrons," J. Phys. B **48**, 214003 (2015).
9. Y. Matsuoka, Y. Kizuka, and T. Inoue, "The characteristics of laser micro drilling using a Bessel beam," Appl. Phys. A **84**, 423–430 (2006).
10. M. Duocastella and C. Arnold, "Bessel and annular beams for materials processing," Laser Photonics Rev. **6**, 607–621 (2012).
11. K.-S. Lee and J. P. Rolland, "Bessel beam spectral-domain high-resolution optical coherence tomography with micro-optic axicon providing extended focusing range," Opt. Lett. **33**, 1696–1698 (2008).
12. L. Yi, L. Sun, and W. Ding, "Multifocal spectral-domain optical coherence tomography based on Bessel beam for extended imaging depth," J. Biomed. Opt. **22**, 106016 (2017).
13. D. McGloin, V. Garcés-Chávez, and K. Dholakia, "Interfering Bessel beams for optical micromanipulation," Opt. Lett. **28**, 657–659 (2003).
14. J. D. Heebl, M. Ettorre, and A. Grbic, "Wireless links in the radiative near field via Bessel beams," Phys. Rev. Appl. **6**, 034018 (2016).
15. V. Garcés-Chávez, D. McGloin, H. Melville, W. Sibbett, and K. Dholakia, "Simultaneous micromanipulation in multiple planes using a self-reconstructing light beam," Nature **419**, 145–147 (2002).
16. A. Gatto, M. Tacca, P. Martelli, P. Boffi, and M. Martinelli, "Free-space orbital angular momentum division multiplexing with Bessel beams," J. Opt. **13**, 064018 (2011).
17. N. Bozinovic, Y. Yue, Y. Ren, M. Tur, P. Kristensen, H. Huang, A. E. Willner, and S. Ramachandran, "Terabit-scale orbital angular momentum mode division multiplexing in fibers," Science **340**, 1545–1548 (2013).
18. J. Wang, J.-Y. Yang, I. M. Fazal, N. Ahmed, Y. Yan, H. Huang, Y. Ren, Y. Yue, S. Dolinar, M. Tur, and A. E. Willner, "Terabit free-space data transmission employing orbital angular momentum multiplexing," Nat. Photonics **6**, 488–496 (2012).
19. Y. Yan, G. Xie, M. P. J. Lavery, H. Huang, N. Ahmed, C. Bao, Y. Ren, Y. Cao, L. Li, Z. Zhao, A. F. Molisch, M. Tur, M. J. Padgett, and A. E. Willner, "High-capacity millimetre-wave communications with orbital angular momentum multiplexing," Nat. Commun. **5**, 4876 (2014).
20. C. Vetter, T. Eichelkraut, M. Ornigotti, and A. Szameit, "Generalized radially self-accelerating helicon beams," Phys. Rev. Lett. **113**, 183901 (2014).
21. C. Vetter, T. Eichelkraut, M. Ornigotti, and A. Szameit, "Optimization and control of two-component radially self-accelerating beams," Appl. Phys. Lett. **107**, 211104 (2015).
22. M. Ornigotti and A. Szameit, "Radially self-accelerating optical pulses," Phys. Rev. A **99**, 023859 (2019).
23. G. Scott and N. McArdle, "Efficient generation of nearly diffraction-free beams using an axicon," Opt. Eng. **31**, 2640–2643 (1992).
24. A. Vasara, J. Turunen, and A. T. Friberg, "Realization of general nondiffracting beams with computer-generated holograms," J. Opt. Soc. Am. A **6**, 1748–1754 (1989).
25. C. Lyu, M. R. Belic, Y. Li, and Y. Zhang, "Generation of diffraction-free Bessel beams based on combined axicons," Opt. Laser Technol. **164**, 109548 (2023).

26. A. J. Asuncion and R. A. Guerrero, "Generating superimposed Bessel beams with a volume holographic axicon," Appl. Opt. **56**, 4206–4212 (2017).
27. Q. Feng, Y. Lin, M. Shan, Y. Mu, and L. Li, "Generation and measurement of a Bessel vortex beam carrying multiple orbital-angular-momentum modes through a reflective metasurface in the RF domain," Phys. Rev. Appl. **15**, 064044 (2021).
28. J. Wen, L. Chen, X. Chen, S. Kanwal, L. Zhang, S. Zhuang, D. Zhang, and D. Lei, "Use of dielectric metasurfaces to generate deep-subwavelength nondiffractive Bessel-like beams with arbitrary trajectories and ultralarge deflection," Laser Photonics Rev. **15**, 2000487 (2021).
29. X. Meng, X. Chen, R. Chen, H. Li, T. Qu, and A. Zhang, "Generation of multiple high-order Bessel beams carrying different orbital-angular-momentum modes through an anisotropic holographic impedance metasurface," Phys. Rev. Appl. **16**, 044063 (2021).
30. N. Jiménez, R. Picó, V. Sánchez-Morcillo, V. Romero-García, L. M. García-Raffi, and K. Staliunas, "Formation of high-order acoustic Bessel beams by spiral diffraction gratings," Phys. Rev. E **94**, 053004 (2016).
31. C. Vetter, R. Steinkopf, K. Bergner, M. Ornigotti, S. Nolte, H. Gross, and A. Szameit, "Realization of free-space long-distance self-healing Bessel beams," Laser Photonics Rev. **13**, 1900103 (2019).
32. N. Chattrapiban, E. A. Rogers, D. Cofield, I. Wendell, T. Hill, and R. Roy, "Generation of nondiffracting Bessel beams by use of a spatial light modulator," Opt. Lett. **28**, 2183–2185 (2003).
33. S. H. Tao, W. M. Lee, and X.-C. Yuan, "Dynamic optical manipulation with a higher-order fractional Bessel beam generated from a spatial light modulator," Opt. Lett. **28**, 1867–1869 (2003).
34. J. Wu, Z. Wu, Y. He, A. Yu, Z. Zhang, Z. Wen, and G. Chen, "Creating a nondiffracting beam with sub-diffraction size by a phase spatial light modulator," Opt. Express **25**, 6274–6282 (2017).
35. R. Bowman, N. Muller, X. Zambrana-Puyalto, O. Jedrkiewicz, P. Di Trapani, and M. J. Padgett, "Efficient generation of Bessel beam arrays by means of an SLM," Eur. Phys. J. Spec. Top. **199**, 159–166 (2011).
36. Y. Ni, C. Chen, S. Wen, *et al.*, "Computational spectropolarimetry with a tunable liquid crystal metasurface," eLight **2**, 23 (2022).
37. J. Yim, N. Chandra, X. Feng, *et al.*, "Broadband continuous supersymmetric transformation: a new paradigm for transformation optics," eLight **2**, 16 (2022).
38. Z. Jin, D. Janoschka, J. Deng, *et al.*, "Phyllotaxis-inspired nanosieves with multiplexed orbital angular momentum," eLight **1**, 5 (2021).
39. M. Wang, G. Hu, S. Chand, *et al.*, "Spin-orbit-locked hyperbolic polariton vortices carrying reconfigurable topological charges," eLight **2**, 12 (2022).
40. L. Zhu and J. Wang, "Arbitrary manipulation of spatial amplitude and phase using phase-only spatial light modulators," Sci. Rep. **4**, 7441 (2014).
41. J. A. Davis, J. Guertin, and D. M. Cottrell, "Diffraction-free beams generated with programmable spatial light modulators," Appl. Opt. **32**, 6368–6370 (1993).
42. W. T. Chen, M. Khorasaninejad, A. Y. Zhu, J. Oh, R. C. Devlin, A. Zaidi, and F. Capasso, "Generation of wavelength-independent subwavelength Bessel beams using metasurfaces," Light Sci. Appl. **6**, e16259 (2017).
43. Z. Wang, S. Dong, W. Luo, M. Jia, Z. Liang, Q. He, S. Sun, and L. Zhou, "High-efficiency generation of Bessel beams with transmissive metasurfaces," Appl. Phys. Lett. **112**, 191901 (2018).
44. J. Li, Y. Yuan, Y. Wang, S. Yang, Q. Wu, and K. Zhang, "Generating Bessel beams efficiently in microwave with high transmission metasurfaces," IEEE Trans. Magn. **57**, 2500805 (2021).
45. D. Lee, S. So, G. Hu, *et al.*, "Hyperbolic metamaterials: fusing artificial structures to natural 2D materials," eLight **2**, 1 (2022).
46. L. Li, H. Zhao, C. Liu, *et al.*, "Intelligent metasurfaces: control, communication and computing," eLight **2**, 7 (2022).
47. N. K. Efremidis, Z. Chen, M. Segev, and D. N. Christodoulides, "Airy beams and accelerating waves: an overview of recent advances," Optica **6**, 686–701 (2019).